Advanced Composite Materials
Publication details, including instructions for authors and subscription information:
http://www.tandfonline.com/loi/tacm20

Analysis of filament-wound sandwich pipe under internal pressure

M. Xia , K. Kemmochi & H. Takayanagi

Version of record first published: 02 Apr 2012.

To cite this article: M. Xia , K. Kemmochi & H. Takayanagi (2000): Analysis of filament-wound sandwich pipe under internal pressure, Advanced Composite Materials, 9:3, 223-239

To link to this article: http://dx.doi.org/10.1163/15685510051033403

Adv. Composite Mater., Vol. 9, No. 3, pp. 223–239 (2000)

Analysis of filament-wound sandwich pipe under internal pressure

M. XIA, K. KEMMOCHI and H. TAKAYANAGI

National Institute of Materials and Chemical Research, Agency of Industrial Science and Technology, MITI, 1-1, Higashi, Tsukuba, Ibaraki 305-8565, Japan

Received 22 January 2000; accepted 14 February 2000

Abstract—Using the classical laminated plate theory, a computer model has been developed to investigate stresses and strains of thick-walled sandwich pipes under internal pressure. The sandwich pipe is created using non-reinforced material for the core layer and an alternate-ply material for the skin layers. Considering the complicated material properties of the skin layers reinforced by alternate-ply composites, the analysis is based on treating typical sandwich pipes that are three-dimensional, cylindrical, and orthotropic. The computer model conducts stress and strain analysis of sandwich pipe with different winding angles. The optimum winding angles have been found to be in the 60° range, and the strength of the sandwich pipe has been found to decrease rapidly when the core layer modulus is less than 20 GPa.

Keywords: Orthotropic analysis; sandwich cylindrical pipe; internal pressure; alternate-ply material.

1. INTRODUCTION

Recently, there has been a growing interest in developing fiber-reinforced cylindrical composite structures. As filament-wound pipes made of fiber-reinforced plastics have many potential advantages over pipes made from conventional materials, a number of investigations to characterize failure mechanisms of filament-wound pipes have been conducted. For thin-walled cylindrical-pressure vessels with a ratio of applied hoop-to-axial stress of two to one, an optimum winding angle of 55° was noted, and many experimental failure analyses were conducted for filament-wound pipe with a 55°-winding angle [1–4]. Rosenow [5] used the classical laminated plate theory to predict the stress and strain response of pipes with winding angles varying from 15° to 85°, and he compared them with experimental results. A 55°-winding angle was shown to be optimum for the hoop-to-axial stress ratio of two, but the optimum angle had to be about 75° in the case of pressure without axial loading. Spencer and Hull [6] and Uemura and Fukunaga [7] have investigated, respectively, the failure mechanism in CFRP and GFRP pipes wound at different

winding angles. The maximum weepage stress was found to be around 55°, and negative axial strains were observed within a range of 35° to 50°. Wild and Vickers [8] have developed an analytical procedure based on the theory of orthotropic cylindrical sheets and modeled both plane stress and plane strain states of cylindrical sheets comprising a number of cylindrical sublayers, each of which is cylindrically orthotropic. The optimum winding angle was shown to play an important part in the design of filament-wound cylindrical shells.

Most previous studies on cylindrical fiber-reinforced composite structures have focused on thin-walled cylindrical shells. However, only limited studies have been published dealing with thick-walled cylindrical pipe behaviors [9–13]. Roy [9] presented a thermal stress analysis of a thick laminated ring assumed to be cylindrically orthotropic. The analysis was based on treating the ring with orthotropic materials in the state of plane stress in the hoop and axial ($\theta - r$) plane. Ben [10] has reported an accurate, finite-cylindrical element method to obtain thermal stresses and the deformation for thick-walled cylindrical pipes. In his work, the effects of thermal residual stresses on the design of thick-walled FRP cylindrical pipes were discussed. Ben did not consider axial loading of cylinders with closed ends in his mechanical analyses of cylindrical pipes under internal pressure. In recent years, a finite element method has become available for use in analyzing mechanical behaviors of cylindrical fiber-reinforced composite structures [11, 12]. Kitao and Akiyama [13] have analyzed and evaluated the progress of failure in thick-walled FW pipes with different winding-angles under internal pressure. Using the finite Hankel transform and the Laplace transform, the elastodynamic solution for the thermal shock stresses in an orthotropic thick cylindrical shell has been reported by Cho *et al*. [14]. The concept of an elastic–plastic stress field was predicted in a coated-continuous fibers composite subjected to thermomechanical loading by You *et al*. [15].

Sandwich composite pipes, composed of two skin layers and a core layer, can be suitably tailored to give optimum material properties by making effective use of each material property in the moldings. There are few investigations on the mechanical properties of sandwich pipes, and almost no literature reports on the stress and the deformation analysis of sandwich composite pipes. We attempt to provide an analytical foundation for the investigation of stress and deformation in a filament-wound sandwich pipe under internal pressure. Especially, considering the complicated material properties of the skin layers reinforced by alternate-ply composites, our analysis is based on treating typical sandwich pipes that are three-dimensional, cylindrical, and orthotropic. With our computer model, we conducted stress and strain analysis of the sandwich pipe using different winding angles.

2. STRESS ANALYSIS

The sandwich pipe is created using non-reinforced materials for the core layer and alternate-ply materials for the skin layers. The alternate-ply skin layers are those in which the principal material directions of the adjacent layer have an opposite fiber

orientation ($\pm\theta$) with respect to the axial direction. The adjacent two lay-ups are assumed here to behave together as an orthotropic unit. In this paper, the orthotropic unit of the lay-up angle ($\pm\theta$) is referred to as an orthotropic layer of angle θ. Figures 1 and 2 show the cylindrical coordinates and configuration notations for the sandwich pipe.

2.1. Transformation from ply properties to laminate properties

Using the cylindrical coordinate system shown in Fig. 1, the stress and strain transformation of the kth layer with the orthotropic alternate-ply material is given by

$$\begin{bmatrix} \sigma_r \\ \sigma_\theta \\ \sigma_z \end{bmatrix}^{(k)} = \begin{bmatrix} C_{11} & C_{12} & C_{13} \\ C_{12} & C_{22} & C_{23} \\ C_{13} & C_{23} & C_{33} \end{bmatrix}^{(k)} \begin{bmatrix} \varepsilon_r \\ \varepsilon_\theta \\ \varepsilon_z \end{bmatrix}^{(k)} . \tag{1}$$

Based upon the classical laminated-plate theory, the matrix $[C_{ij}]$ in equation (1) can be written as equation (2) by using the stiffness transformation matrix of the coordinate system between the on-axis and the cylindrical axis shown in Fig. 3.

$$\begin{bmatrix} C_{33} \\ C_{23} \\ C_{13} \\ C_{22} \\ C_{12} \\ C_{11} \end{bmatrix}^{(k)} = \begin{bmatrix} m^4 & n^4 & 0 & 2m^2n^2 & 0 & 0 & 4m^2n^2 \\ m^2n^2 & m^2n^2 & 0 & m^4+n^4 & 0 & 0 & -4m^2n^2 \\ 0 & 0 & 0 & 0 & m^2 & n^2 & 0 \\ n^4 & m^4 & 0 & 2m^2n^2 & 0 & 0 & 4m^2n^2 \\ 0 & 0 & 0 & 0 & n^2 & m^2 & 0 \\ 0 & 0 & 1 & 0 & 0 & 0 & 0 \end{bmatrix} \begin{bmatrix} C_{xx} \\ C_{yy} \\ C_{zz} \\ C_{xy} \\ C_{xz} \\ C_{yz} \\ G_{zz} \end{bmatrix}^{(k)} , \tag{2}$$

where $m = \cos\theta$ and $n = \sin\theta$, and θ is the cylindrical angle of the filaments from the pipe axis.

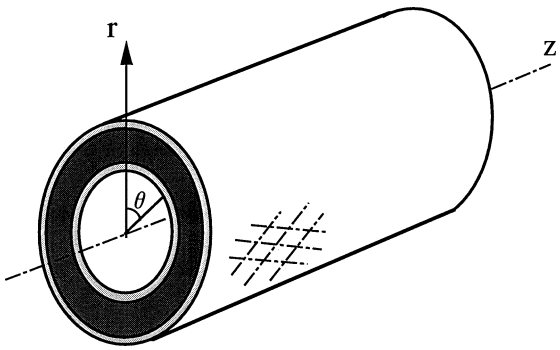

Figure 1. Filament-wound sandwich pipe in cylindrical coordinates.

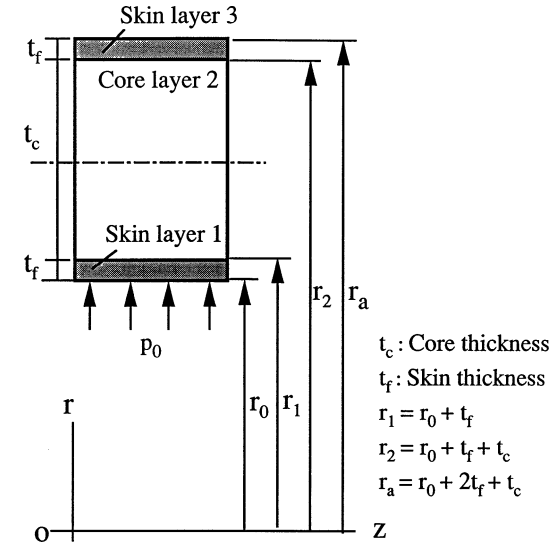

Figure 2. Cross-section of the sandwich pipe.

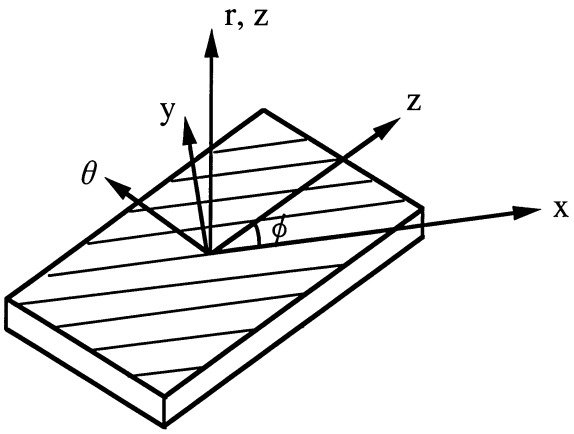

Figure 3. Relation of coordinate system between principal material axis and cylindrical axes.

2.2. 3D alternate-ply properties

To define the three-dimensional alternate-ply material properties, the material modulus matrix elements C_{ij} $(i, j = x, y, z)$ and G_{zz} in equation (2) are needed. Their values can be calculated from engineering constants, defined by

$$E_x, E_y, E_z, \nu_{xy}, \nu_{zx}, \nu_{zy}, G_{xx}, G_{yy}, G_{zz}.$$

For the most general case of orthotropic ply-oriented properties, these values would have to be experimentally measured or estimated using micromechanics. For unidirectional orientation fiber composites, the fiber distributions are very similar in the y and z directions. Therefore, assuming transverse isotropy, and based on equivalent properties in the $y-z$ plane for unidirectional material, we get

$$\begin{aligned} E_y &= E_z, \\ G_{yy} &= G_{zz}, \\ \nu_{zx} &= \nu_{yx}, \end{aligned}$$

where x and y refer to material principal axes along fiber and transverse directions, respectively.

The conversions of engineering constants to modulus matrix elements are obtained from

$$\begin{aligned} &\Delta = S_{xx}S_{yy}S_{zz} + 2S_{xy}S_{yz}S_{xz} - S_{yy}S_{xz}^2 - S_{xx}S_{yz}^2 - S_{zz}S_{xy}^2, \\ &C_{xx} = \left(S_{yy}S_{zz} - S_{yz}^2\right)/\Delta, \quad C_{xy} = \left(S_{xz}S_{yz} - S_{xy}S_{zz}\right)/\Delta, \\ &C_{yy} = \left(S_{xx}S_{zz} - S_{xz}^2\right)/\Delta, \quad C_{xz} = \left(S_{xy}S_{yz} - S_{xz}S_{yy}\right)/\Delta, \\ &C_{zz} = \left(S_{xx}S_{yy} - S_{xy}^2\right)/\Delta, \quad C_{yz} = \left(S_{xy}S_{xz} - S_{xx}S_{yz}\right)/\Delta, \end{aligned} \tag{3}$$

where

$$\begin{aligned} &S_{xx} = 1/E_x, \quad S_{xy} = -\nu_{yx}/E_x, \\ &S_{yy} = 1/E_y, \quad S_{xz} = -\nu_{yx}/E_x, \\ &S_{zz} = 1/E_y, \quad S_{yz} = -\nu_{zy}/E_x. \end{aligned} \tag{4}$$

2.3. Analysis procedure

The equation of equilibrium with circular symmetry is obtained from

$$\frac{\mathrm{d}\sigma_r^{(k)}}{\mathrm{d}r} + \frac{\sigma_r^{(k)} - \sigma_\theta^{(k)}}{r} = 0. \tag{5}$$

The radial and hoop strains, $\varepsilon_r^{(k)}$ and $\varepsilon_\theta^{(k)}$, can be given in the radial displacement $u_r^{(k)}$,

$$\varepsilon_r^{(k)} = \frac{\mathrm{d}u_r^{(k)}}{\mathrm{d}r} \quad \text{and} \quad \varepsilon_\theta^{(k)} = \frac{u_r^{(k)}}{r}. \tag{6}$$

The axial strains $\varepsilon_z^{(k)}$ of all layers are equal to a constant, ε_0.

The stresses $\sigma_r^{(k)}$, $\sigma_\theta^{(k)}$, and $\sigma_z^{(k)}$ can be expressed in terms of strains from equation (1), written as

$$\begin{aligned} \sigma_r^{(k)} &= C_{11}^{(k)}\varepsilon_r^{(k)} + C_{12}^{(k)}\varepsilon_\theta^{(k)} + C_{13}^{(k)}\varepsilon_0, \\ \sigma_\theta^{(k)} &= C_{12}^{(k)}\varepsilon_r^{(k)} + C_{22}^{(k)}\varepsilon_\theta^{(k)} + C_{23}^{(k)}\varepsilon_0, \\ \sigma_z^{(k)} &= C_{13}^{(k)}\varepsilon_r^{(k)} + C_{23}^{(k)}\varepsilon_\theta^{(k)} + C_{33}^{(k)}\varepsilon_0. \end{aligned} \tag{7}$$

Substituting the expressions for the stress in equation (5) and using equation (6), we get

$$\frac{\mathrm{d}^2 u_r^{(k)}}{\mathrm{d}r^2} + \frac{1}{r}\frac{\mathrm{d}u_r^{(k)}}{\mathrm{d}r} - \frac{C_{22}^{(k)}/C_{11}^{(k)}}{r^2} u_r^{(k)} = \frac{\alpha^{(k)}\varepsilon_0}{r}, \tag{8}$$

where $\alpha^{(k)} = (C_{23}^{(k)} - C_{13}^{(k)})/C_{11}^{(k)}$.

When $C_{22}^{(k)}/C_{11}^{(k)} > 0$, if $\beta^{(k)} = \sqrt{C_{22}^{(k)}/C_{11}^{(k)}}$, the solution for equation (8) can be obtained under the following two conditions:
If $\beta^{(k)} \neq 1$ (anisotropic)

$$u_r^{(k)} = A^{(k)} r^{\beta^{(k)}} + B^{(k)} r^{-\beta^{(k)}} + \frac{\alpha^{(k)}\varepsilon_0 r}{1 - (\beta^{(k)})^2}. \tag{9}$$

If $\beta^{(k)} = 1$ (isotropic or isotropic in $-\theta(r)$ planer)

$$u_r^{(k)} = \frac{\alpha^{(k)}\varepsilon_0 r}{2} \ln r + A^{(k)} r + B^{(k)}/r. \tag{10}$$

When $C_{22}^{(k)}/C_{11}^{(k)} < 0$, if $\beta^{(k)} = \sqrt{-C_{22}^{(k)}/C_{11}^{(k)}}$

$$u_r^{(k)} = A^{(k)} \cos\left(\beta^{(k)} \ln r\right) + B^{(k)} \sin\left(\beta^{(k)} \ln r\right) + \frac{\alpha^{(k)}\varepsilon_0 r}{1 + (\beta^{(k)})^2}, \tag{11}$$

here, $A^{(k)}$ and $B^{(k)}$ are unknown constants of integration, which are to be determined from the boundary conditions and the contact conditions at each interface between the core and skin layers.

Assuming the interfaces between the core and skin layers are perfectly bound, the continuance of displacements and tractions along the interfaces and traction-free boundary conditions provides a homogeneous equation.

The traction condition (pressure p_0) at the inner surface and the traction-free condition at the outer surface are written as

$$\begin{aligned} \sigma_r^{(1)}(r_0) &= -p_0, \\ \sigma_r^{(n)}(r_a) &= 0, \end{aligned} \tag{12}$$

where r_0 and r_a are the inner and outer radii, respectively.

Continuity of transactions leads to

$$\begin{aligned} u_r^{(k)}(r_k) &= u_r^{(k+1)}(r_k), \quad k = 1, 2, \ldots, n, \\ \sigma_r^{(k)}(r_k) &= \sigma_r^{(k+1)}(r_k), \quad k = 1, 2, \ldots, n. \end{aligned} \tag{13}$$

For a cylinder with closed ends, the axial equilibrium is satisfied by the following relation:

$$2\pi \sum_{k=1}^{n} \int_{r_{k-1}}^{r_k} \sigma_z^{(k)}(r) r \, \mathrm{d}r = \pi r_0^2 p_0. \tag{14}$$

Equations (12)–(14) can give a set of equations to determine unknown constants $A^{(k)}$, $B^{(k)}$, and axial strain ε_0. The simultaneous equation, for the sandwich pipe ($n = 3$) shown in Fig. 2, can be written as follows:

$$\begin{bmatrix} k_{11} & k_{12} & k_{13} & k_{14} & k_{15} & k_{16} & k_{17} \\ k_{21} & k_{22} & k_{23} & k_{24} & k_{25} & k_{26} & k_{27} \\ k_{31} & k_{32} & k_{33} & k_{34} & k_{35} & k_{36} & k_{37} \\ k_{41} & k_{42} & k_{43} & k_{44} & k_{45} & k_{46} & k_{47} \\ k_{51} & k_{52} & k_{53} & k_{54} & k_{55} & k_{56} & k_{57} \\ k_{61} & k_{62} & k_{63} & k_{64} & k_{65} & k_{66} & k_{67} \\ k_{71} & k_{72} & k_{73} & k_{74} & k_{75} & k_{76} & k_{77} \end{bmatrix} \begin{bmatrix} A^{(1)} \\ A^{(2)} \\ A^{(3)} \\ B^{(1)} \\ B^{(2)} \\ B^{(3)} \\ \varepsilon_0 \end{bmatrix} = \begin{bmatrix} d_1 \\ d_2 \\ d_3 \\ d_4 \\ d_5 \\ d_6 \\ d_7 \end{bmatrix}, \tag{15}$$

where k_{ij} and d_j $(i, j = 1, \ldots, 7)$ in two conditions of $C_{22}^{(k)}/C_{11}^{(k)} > 0$ and $C_{22}^{(k)}/C_{11}^{(k)} < 0$, are given in the Appendix.

Once values of $A^{(k)}$, $B^{(k)}$ $(k = 1, 2, 3)$, and ε_0 obtained from equation (15) are known, the stresses and displacements are thus determined from equations (6)–(11).

3. NUMERICAL RESULTS AND DISCUSSION

A computer procedure based on the above analysis has been incorporated into a FORTRAN program that allows user input of geometric parameters and material properties for the core and skin layers and of the internal pressure load. The program can calculate stress, strain, and deformation of filament-wound sandwich pipes.

The procedure is applied to an example of a composite sandwich pipe with an isotropic-core layer and orthotropic-skin layers. The configuration notation of the sandwich pipe is shown in Fig. 2, which has an inner radius of 50 mm, a core-layer thickness of 20 mm, and a 2 mm skin-layer thickness. In the present study, the first and third skin layers of the sandwich pipe have the same material, which is based on a graphite and epoxy composite (AS4/3501-6) [16]. The engineering constants of (AS4/3501-6) and the isotropic material property for the core layer are given in Table 1.

Netting analysis is a simplified approach to the design of cylindrical filament-wound structures under internal pressure loading. Netting analysis assumes that all

Table 1.
Material properties of AS4/3501-6 and resin

Properties	AS4/3501-6	Resin (core)
E_x (GPa)	138	5.0
E_y (GPa)	8.9	↑
G_{zz} (GPa)	5.17	1.92
ν_{yx}	0.3	0.3
ν_{zy}	0.54	↑

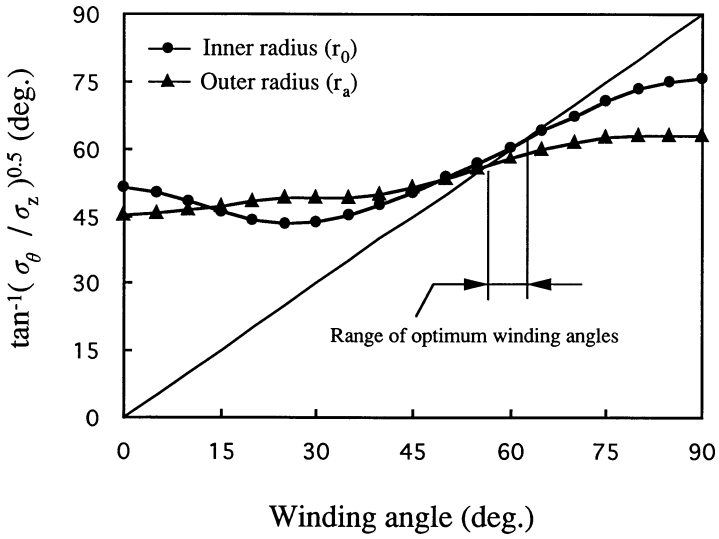

Figure 4. Map of optimum winding angles.

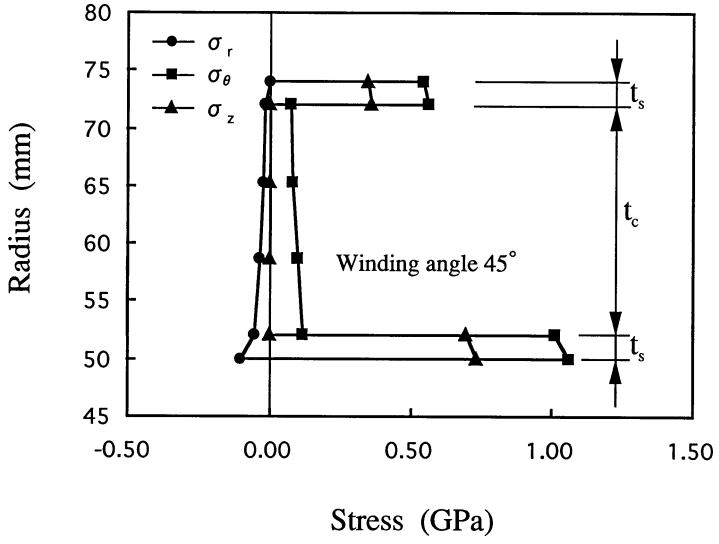

Figure 5. Stress distributions within a sandwich pipe.

strength and stiffness properties are derived from the fibers alone and no forces are transmitted by resin. The analysis gives the optimum winding angle written as

$$\alpha_{\text{opt}} = \tan^{-1}\sqrt{\frac{\sigma_\theta}{\sigma_z}}. \tag{16}$$

For a thin-walled pressure cylinder with closed ends, the ratio of hoop-to-axial stress is equal to two. Using equation (16), the optimal winding angle α_{opt} equal

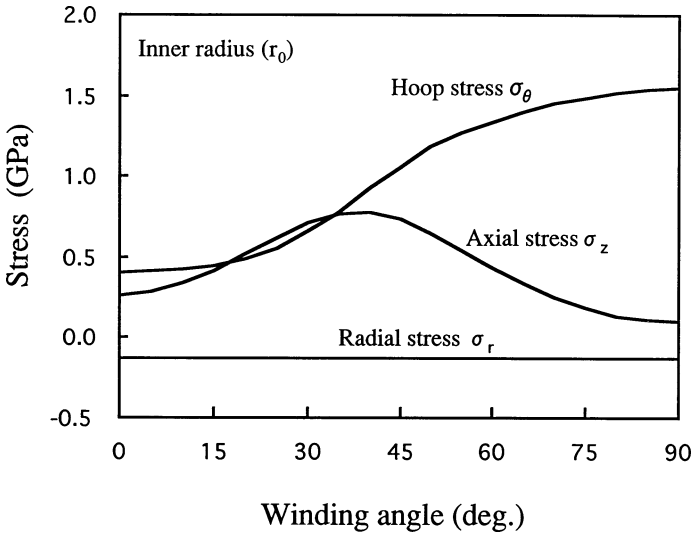

Figure 6. Effect of winding angle on hoop, axial, and radial stress behaviors at inner radius.

to 54.7°. In Hull's paper [4], he described the deformation and failure modes in glass-reinforced polyester pipe wound at 55°. They have tested pipes wound at 55° and have shown that this angle was an optimum winding angle.

With the exception of a thin-walled laminate-ply cylinder, the stress distribution through the wall of a filament-wound cylinder will not be uniform. The ratio of hoop-to-axial stress will also vary with the winding angle.

Figure 4 shows the curves of $\alpha_{\text{opt}} = \tan^{-1}(\sigma_\theta/\sigma_z)^{0.5}$ given by equation (16) varying with the winding angles. The optimal winding angles, which are on the crossings of curves and a straight line, can be obtained from Fig. 4. The optimum winding angles for the inner and the outer layers are very similar, and the values have been shown in the range of around 60°.

The analysis of the sandwich pipe was carried out under the internal pressure of 0.1 GPa. Figure 5 shows the axial, hoop, and radial stress distribution through the wall of the sandwich pipe with a 45°-winding angle. The values of stress distributions are larger at the inner radius than at the outer radius. The skin layers are subjected to higher stresses compared to the core layer. Therefore, it is safe to predict that the first failure mode for the sandwich pipe will occur on the inner skin layer.

The hoop, axial, and radial stress curves varying with the winding angles at the inner and outer radii are shown in Figs 6 and 7, respectively. The hoop and axial stresses for the thick-walled pipe vary with the winding angle. Both the hoop and the axis are subjected to tensile stresses, and the difference of stresses between the hoop and axial directions increases rapidly when the winding angle is greater than 35°. The strain curve in the axial direction and the strain curves in the hoop and the radial directions varying with the winding angle are shown in Figs 8 and 9,

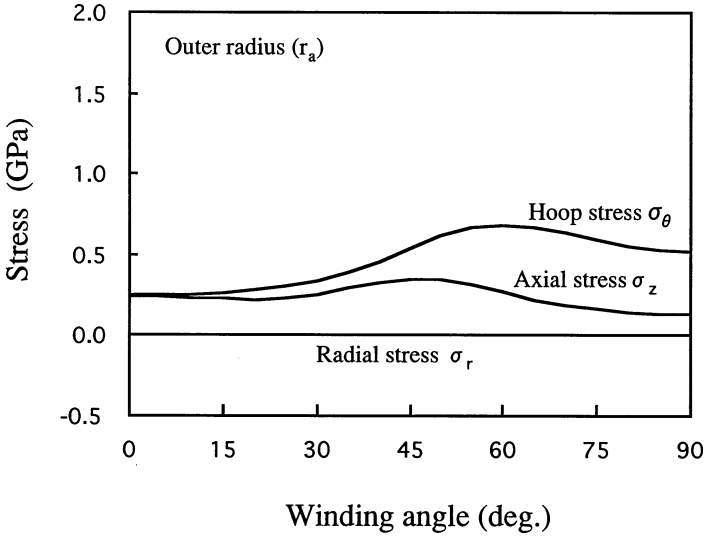

Figure 7. Effect of winding angle on hoop, axial, and radial stress behaviors at outer radius.

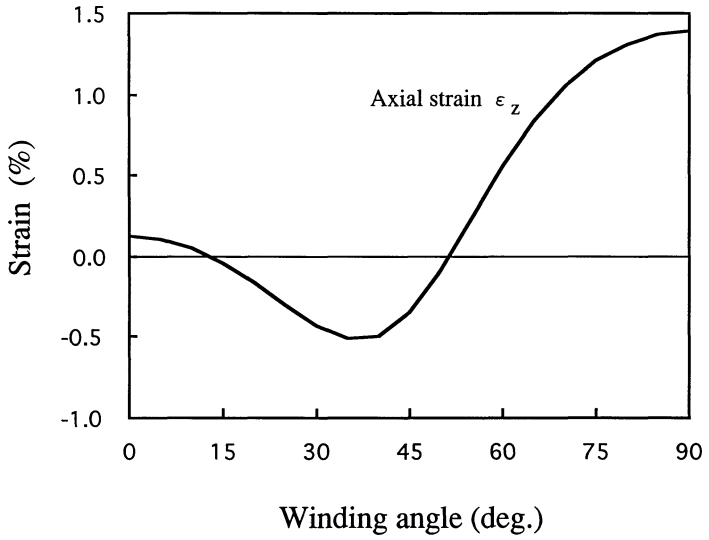

Figure 8. Effect of winding angle on axial strain behavior.

respectively. The axial strain of the cylinder under inner pressure must be greater than zero for the isotropic sandwich pipe. Figure 8 shows that the axial strain is negative within a 15° to 50° range of winding angles because of the effect of the anisotropic elasticity on the axial strain. This result has also been obtained in other experiments [6, 7]. Figure 9 shows that the radial strains are larger at the inner than at the outer radius.

The influence of the core material on the hoop stress with a 60°-winding angle is shown in Fig. 10. The hoop stress decreases while increasing the modulus of the

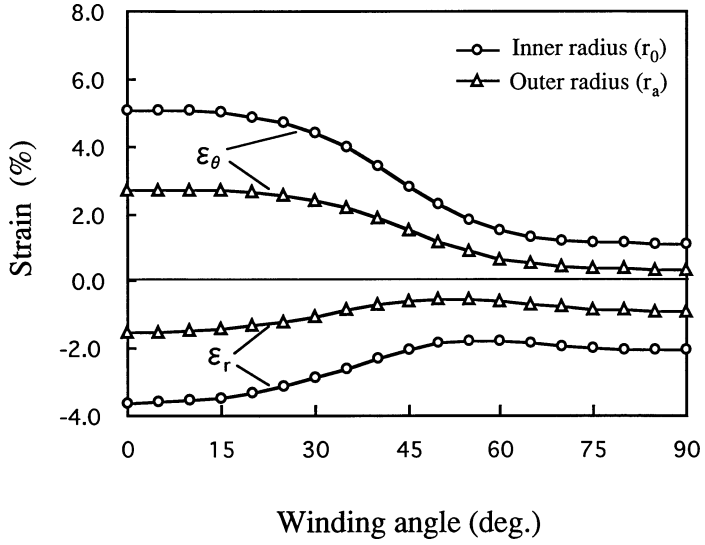

Figure 9. Effect of winding angle on hoop and radial strain behaviors.

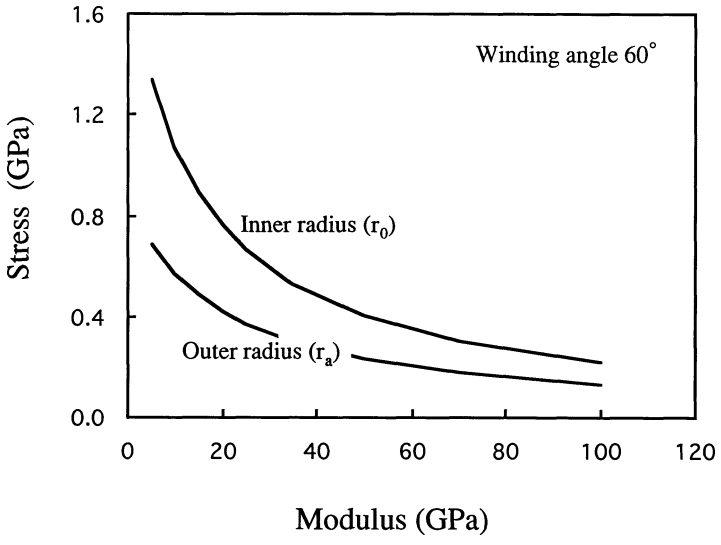

Figure 10. Effect of core stiffness on hoop-stress behavior.

core layer. The effect of the core material on the hoop stress at the outer radius is less sensitive than that at the inner radius. The difference of the hoop stress between the inner and outer radii becomes smaller when the modulus of the core layer is increased. This is because the core layer material with a high degree of stiffness intensifies the transfer of the force due to the internal pressure from the inner to outer layers. The influence of the core material on the hoop stress becomes weak when the core layer modulus is larger than 20 GPa.

4. CONCLUSIONS

An analytical procedure is developed to assess stresses and strains of the filament-wound sandwich pipe due to internal pressure. This procedure is based on the classical laminated plate theory. The sandwich pipe is considered in 3D analysis and in an orthotropic-material model. The analytical procedure developed here provides a basis for describing the elastic behavior of the filament-wound sandwich pipe.

The winding angle of the filaments varies, depending upon geometry and construction materials. The optimum winding angles are obtained from netting analysis, which gives a range of around 60°. For the thick-walled laminate-ply sandwich pipe, a 55°-winding angle is no longer an optimum arrangement.

In the analytical results, the axial strain changes from positive to negative with respect to the winding angle. Because the core layer with a high degree of stiffness intensifies the connection between the inner and outer layers, both hoop stress and the difference of stress between the inner and outer layers decrease while increasing the modulus of the core layer.

REFERENCES

1. P. D. Soden, R. Kitching and P. C. Tse, Experimental failure stresses for ±55° filament wound glass fiber reinforced plastic tubes under biaxial loads, *Composites* **20**, 125–135 (1989).
2. P. D. Soden, D. Leadbetter, P. R. Griggs and G. C. Eckold, The strength of a filament wound composite under biaxial loading, *Composites* **9**, 247–250 (1978).
3. J. Mistry, A. G. Gibson and Y.-S. Wu, Failure of composite cylinders under combined external pressure and axial loading, *Compos. Struct.* **22**, 193–200 (1992).
4. D. Hull, M. J. Legg and B. Spencer, Failure of glass/polyester filament wound pipe, *Composites* **9**, 17–24 (1978).
5. M. W. K. Rosenow, Wind angle of effects in glass fiber-reinforced polyester filament wound pipes, *Composites* **15**, 144–152 (1984).
6. B. Spencer and D. Hull, Effect of winding angle on the failure of filament wound pipe, *Composites* **9**, 263–271 (1978).
7. M. Uemura and H. Fukunaga, Probabilistic burst strength of filament-wound cylinders under internal pressure, *J. Compos. Mater.* **15**, 462–480 (1981).
8. P. M. Wild and G. W. Vickers, Analysis of filament-wound cylindrical shells under combined centrifugal pressure and axial loading, *Composites* **Part A 28**, 47–55 (1997).
9. A. K. Roy, Response of thick laminated composite rings to thermal stress, *Compos. Struct.* **18**, 125–139 (1991).
10. G. Ben, Structural analyses of thick-walled cross-ply laminated FRP cylindrical shells, *Trans. Jpn. Soc. Mech. Eng.* **Part A 57**, 1412–1417 (1991) (in Japanese).
11. K. Kim and G. Z. Voyiadjis, Buckling strength prediction of CFRP cylindrical panels using finite element method, *Composites* **Part A 30**, 1093–1104 (1999).
12. J. H. Kweon, Post-failure analysis of composite cylindrical panels under compression, *J. Rein. Plas. Compos.* **17**, 1665–1681 (1998).
13. K. Kitao and H. Akiyama, Failure of thick-wall filament wound plastic pipes under internal pressure, *J. Soc. Mater. Sci., Japan* **43**, 1134–1140 (1994) (in Japanese).
14. H. Cho, G. A. Kardomateas and C. S. Valle, Elastodynamic solution for the thermal shock stresses in an orthotropic thick cylindrical shell, *ASME Journal of Applied Mechanics* **65**, 184–193 (1998).

15. L. You, S. Long and L. Rohr, Elastic-plastic stress field in a coated continuous fibrous composite subjected to thermomechanical loading, *ASME Journal of Applied Mechanics* **66**, 750–757 (1999).
16. F. G. Yuan and C. C. Hsieh, Three-dimensional wave propagation in composite cylindrical shells, *Compos. Struc.* **42**, 153–167 (1998).

APPENDIX

(1) When $C_{22}^{(k)}/C_{11}^{(k)} > 0$

$$
\begin{aligned}
&k_{11} = \left(\beta^{(1)}C_{11}^{(1)} + C_{12}^{(1)}\right)r_0^{\beta^{(1)}-1},\\
&k_{14} = \left(-\beta^{(1)}C_{11}^{(1)} + C_{12}^{(1)}\right)r_0^{-\beta^{(1)}-1},\\
&k_{17} = \frac{\alpha^{(1)}}{1-(\beta^{(1)})^2}\left[C_{11}^{(1)} + C_{12}^{(1)}\right] + C_{13}^{(1)},\\
&k_{12} = k_{13} = k_{15} = k_{16} = 0,\\
&d_1 = -p_0,
\end{aligned}
$$

$$
\begin{aligned}
&k_{21} = r_1^{\beta^{(1)}}, \quad k_{22} = -r_1, \quad k_{23} = 0,\\
&k_{24} = r_1^{-\beta^{(1)}}, \quad k_{25} = -1/r_1, \quad k_{26} = 0,\\
&k_{27} = \frac{\alpha^{(1)}r_1}{1-(\beta^{(1)})^2} - \frac{\alpha^{(2)}r_1}{2}\ln r_1,\\
&d_2 = 0,
\end{aligned}
$$

$$
\begin{aligned}
&k_{31} = 0, \quad k_{32} = r_2, \quad k_{33} = -r_2^{\beta^{(3)}},\\
&k_{34} = 0, \quad k_{35} = 1/r_2, \quad k_{36} = -r_2^{-\beta^{(3)}},\\
&k_{37} = \frac{\alpha^{(2)}r_2}{2}\ln r_2 - \frac{\alpha^{(3)}r_2}{1-(\beta^{(3)})^2},\\
&d_3 = 0,
\end{aligned}
$$

$$
\begin{aligned}
&k_{41} = \left(\beta^{(1)}C_{11}^{(1)} + C_{12}^{(1)}\right)r_1^{\beta^{(1)}-1},\\
&k_{42} = -\left(C_{11}^{(2)} + C_{12}^{(2)}\right),\\
&k_{44} = \left(-\beta^{(1)}C_{11}^{(1)} + C_{12}^{(1)}\right)r_1^{-\beta^{(1)}-1},\\
&k_{45} = -\left(C_{12}^{(2)} - C_{11}^{(2)}\right)/r_1^2,
\end{aligned}
$$

$$k_{47} = \frac{\alpha^{(1)}}{1-(\beta^{(1)})^2}\left[C_{11}^{(1)} + C_{12}^{(1)}\right] + C_{13}^{(1)} - \frac{\alpha^{(2)}\ln r_1\left[C_{11}^{(2)} + C_{12}^{(2)}\right] + \alpha^{(2)}C_{11}^{(2)} + 2C_{13}^{(2)}}{2},$$

$$k_{43} = k_{46} = 0,$$

$$d_4 = 0,$$

$$k_{51} = k_{54} = 0,$$

$$k_{52} = C_{11}^{(2)} + C_{12}^{(2)},$$

$$k_{53} = -\left(\beta^{(3)}C_{11}^{(3)} + C_{12}^{(3)}\right)r_2^{\beta^{(3)}-1},$$

$$k_{55} = \left(C_{12}^{(2)} - C_{11}^{(2)}\right)/r_2^2,$$

$$k_{56} = -\left(-\beta^{(3)}C_{11}^{(3)} + C_{12}^{(3)}\right)r_2^{-\beta^{(3)}-1},$$

$$k_{57} = \frac{\alpha^{(2)}\ln r_2\left[C_{11}^{(2)} + C_{12}^{(2)}\right] + \alpha^{(2)}C_{11}^{(2)} + 2C_{13}^{(2)}}{2} - \frac{\alpha^{(3)}}{1-(\beta^{(3)})^2}\left[C_{11}^{(3)} + C_{12}^{(3)}\right] + C_{13}^{(3)},$$

$$d_5 = 0,$$

$$k_{61} = k_{62} = k_{64} = k_{65} = 0,$$

$$k_{63} = \left(\beta^{(3)}C_{11}^{(3)} + C_{12}^{(3)}\right)r_a^{\beta^{(3)}-1},$$

$$k_{66} = \left(-\beta^{(3)}C_{11}^{(3)} + C_{12}^{(3)}\right)r_a^{-\beta^{(3)}-1},$$

$$k_{67} = \frac{\alpha^{(3)}}{1-(\beta^{(3)})^2}\left[C_{11}^{(3)} + C_{12}^{(3)}\right] + C_{13}^{(3)},$$

$$d_6 = 0,$$

$$k_{71} = \frac{2\left(\beta^{(1)}C_{13}^{(1)} + C_{23}^{(1)}\right)}{1+\beta^{(1)}}\left[r_1^{\beta^{(1)}+1} - r_0^{\beta^{(1)}+1}\right],$$

$$k_{72} = \left(C_{13}^{(2)} + C_{23}^{(2)}\right)\left(r_2^2 - r_1^2\right),$$

$$k_{73} = \frac{2\left(\beta^{(3)}C_{13}^{(3)} + C_{23}^{(3)}\right)}{1+\beta^{(3)}}\left[r_a^{\beta^{(3)}+1} - r_2^{\beta^{(3)}+1}\right],$$

$$k_{74} = \frac{2\left(-\beta^{(1)}C_{13}^{(1)} + C_{23}^{(1)}\right)}{1-\beta^{(1)}}\left[r_1^{-\beta^{(1)}+1} - r_0^{-\beta^{(1)}+1}\right],$$

$$k_{75} = 2\left(C_{23}^{(2)} - C_{13}^{(2)}\right)\ln(r_2/r_1),$$

$$k_{76} = \frac{2\left(-\beta^{(3)}C_{13}^{(3)} + C_{23}^{(3)}\right)}{1-\beta^{(3)}}\left[r_a^{-\beta^{(3)}+1} - r_2^{-\beta^{(3)}+1}\right],$$

$$k_{77} = \left[\frac{\alpha^{(1)}\left(C_{13}^{(1)} + C_{23}^{(1)}\right)}{1-(\beta^{(1)})^2} + C_{33}^{(1)}\right]\left(r_1^2 - r_0^2\right)$$
$$+\alpha^{(2)}\left(C_{13}^{(2)} + C_{23}^{(2)}\right)\left[\left(r_2^2 \ln r_2 - r_1^2 \ln r_1\right)/2 - \left(r_2^2 - r_1^2\right)/4\right]$$
$$+\left[\alpha^{(2)}C_{13}^{(2)}/2 + C_{33}^{(2)}\right]\left(r_2^2 - r_1^2\right) + \left[\frac{\alpha^{(3)}[C_{13}^{(3)} + C_{23}^{(3)}]}{1-(\beta^{(3)})^2} + C_{33}^{(3)}\right]\left(r_a^2 - r_2^2\right),$$

$$d_7 = p_0 r_0^2.$$

(2) When $C_{22}^{(k)}/C_{11}^{(k)} < 0$

$$k_{11} = \left[-\beta^{(1)}C_{11}^{(1)}\sin\left(\beta^{(1)}\ln r_0\right) + C_{12}^{(1)}\cos\left(\beta^{(1)}\ln r_0\right)\right]/r_0,$$

$$k_{14} = \left[\beta^{(1)}C_{11}^{(1)}\cos\left(\beta^{(1)}\ln r_0\right) + C_{12}^{(1)}\sin\left(\beta^{(1)}\ln r_0\right)\right]/r_0,$$

$$k_{17} = \frac{\alpha^{(1)}}{1+(\beta^{(1)})^2}\left[C_{11}^{(1)} + C_{12}^{(1)}\right] + C_{13}^{(1)},$$

$$k_{12} = k_{13} = k_{15} = k_{16},$$

$$d_1 = -p_0,$$

$$k_{21} = \cos\left(\beta^{(1)}\ln r_1\right),$$

$$k_{22} = -r_1,$$

$$k_{24} = \sin\left(\beta^{(1)}\ln r_1\right),$$

$$k_{25} = -1/r_1,$$

$$k_{27} = \frac{\alpha^{(1)}r_1}{1+(\beta^{(1)})^2} - \frac{\alpha^{(2)}r_1}{2}\ln r_1,$$

$$k_{23} = k_{26} = 0,$$

$$d_2 = 0,$$

$$k_{31} = k_{34} = 0,$$

$$k_{32} = r_2,$$

$$k_{33} = -\cos\left(\beta^{(3)}\ln r_2\right),$$

$$k_{35} = 1/r_2,$$

$$k_{36} = -\sin\left(\beta^{(3)}\ln r_2\right),$$

$$k_{37} = \frac{\alpha^{(2)} r_2}{2} \ln r_2 - \frac{\alpha^{(3)} r_2}{1 + (\beta^{(3)})^2},$$
$$d_3 = 0,$$

$$k_{41} = \left[-\beta^{(1)} C_{11}^{(1)} \sin\left(\beta^{(1)} \ln r_1\right) + C_{12}^{(1)} \cos\left(\beta^{(1)} \ln r_1\right) \right] / r_1,$$
$$k_{42} = -\left(C_{11}^{(2)} + C_{12}^{(2)} \right),$$
$$k_{44} = \left[\beta^{(1)} C_{11}^{(1)} \cos\left(\beta^{(1)} \ln r_1\right) + C_{12}^{(1)} \sin\left(\beta^{(1)} \ln r_1\right) \right] / r_1,$$
$$k_{45} = -\left(C_{12}^{(2)} - C_{11}^{(2)} \right) / r_1^2,$$
$$k_{47} = \frac{\alpha^{(1)}}{1 + (\beta^{(1)})^2} \left[C_{11}^{(1)} + C_{12}^{(1)} \right] + C_{13}^{(1)} - \frac{\alpha^{(2)} \ln r_1 \left[C_{11}^{(2)} + C_{12}^{(2)} \right] + \alpha^{(2)} C_{11}^{(2)} + 2C_{13}^{(2)}}{2},$$
$$k_{43} = k_{46} = 0,$$
$$d_4 = 0,$$

$$k_{51} = k_{54} = 0,$$
$$k_{52} = C_{11}^{(2)} + C_{12}^{(2)},$$
$$k_{53} = \left[\beta^{(3)} C_{11}^{(3)} \sin\left(\beta^{(3)} \ln r_2\right) - C_{12}^{(3)} \cos\left(\beta^{(3)} \ln r_2\right) \right] / r_2,$$
$$k_{55} = \left(C_{12}^{(2)} - C_{11}^{(2)} \right) / r_2^2,$$
$$k_{56} = -\left[\beta^{(3)} C_{11}^{(3)} \cos\left(\beta^{(3)} \ln r_2\right) + C_{12}^{(3)} \sin\left(\beta^{(3)} \ln r_2\right) \right] / r_2,$$
$$k_{57} = \frac{\alpha^{(2)} \ln r_2 \left[C_{11}^{(2)} + C_{12}^{(2)} \right] + \alpha^{(2)} C_{11}^{(2)} + 2C_{13}^{(2)}}{2} - \frac{\alpha^{(3)}}{1 + (\beta^{(3)})^2} \left[C_{11}^{(3)} + C_{12}^{(3)} \right] + C_{13}^{(3)},$$
$$d_5 = 0,$$

$$k_{61} = k_{62} = k_{64} = k_{65} = 0,$$
$$k_{63} = \left[-\beta^{(3)} C_{11}^{(3)} \sin\left(\beta^{(3)} \ln r_a\right) + C_{12}^{(3)} \cos\left(\beta^{(3)} \ln r_a\right) \right] / r_a,$$
$$k_{66} = \left[\beta^{(3)} C_{11}^{(3)} \cos\left(\beta^{(3)} \ln r_a\right) + C_{12}^{(3)} \sin\left(\beta^{(3)} \ln r_a\right) \right] / r_a,$$
$$k_{67} = \frac{\alpha^{(3)}}{1 + (\beta^{(3)})^2} \left[C_{11}^{(3)} + C_{12}^{(3)} \right] + C_{13}^{(3)},$$
$$d_6 = 0,$$

$$k_{71} = \frac{2}{1+(\beta^{(1)})^2}\Big\{\beta^{(1)}\Big(C_{23}^{(1)} - C_{13}^{(1)}\Big)\Big[r_1\sin\big(\beta^{(1)}\ln r_1\big) - r_0\sin\big(\beta^{(1)}\ln r_0\big)\Big] + \Big(C_{13}^{(1)}(\beta^{(1)})^2 + C_{23}^{(1)}\Big)\Big[r_1\cos\big(\beta^{(1)}\ln r_1\big) - r_0\cos\big(\beta^{(1)}\ln r_0\big)\Big]\Big\},$$

$$k_{72} = \Big(C_{13}^{(2)} + C_{23}^{(2)}\Big)\big(r_2^2 - r_1^2\big),$$

$$k_{73} = \frac{2}{1+(\beta^{(3)})^2}\Big\{\beta^{(3)}\Big(C_{23}^{(3)} - C_{13}^{(3)}\Big)\Big[r_a\sin\big(\beta^{(3)}\ln r_a\big) - r_2\sin\big(\beta^{(3)}\ln r_2\big)\Big] + \Big(C_{13}^{(3)}(\beta^{(3)})^2 + C_{23}^{(3)}\Big)\Big[r_a\cos\big(\beta^{(3)}\ln r_a\big) - r_a\cos\big(\beta^{(3)}\ln r_2\big)\Big]\Big\},$$

$$k_{74} = \frac{2}{1+(\beta^{(1)})^2}\Big\{\Big(C_{13}^{(1)}(\beta^{(1)})^2 + C_{23}^{(1)}\Big)\Big[r_1\sin\big(\beta^{(1)}\ln r_1\big) - r_0\sin\big(\beta^{(1)}\ln r_0\big)\Big] + \beta^{(1)}\Big(C_{13}^{(1)} - C_{23}^{(1)}\Big)\Big[r_1\cos\big(\beta^{(1)}\ln r_1\big) - r_0\cos\big(\beta^{(1)}\ln r_0\big)\Big]\Big\},$$

$$k_{75} = 2\Big(C_{23}^{(2)} - C_{13}^{(2)}\Big)\ln(r_2/r_1),$$

$$k_{76} = \frac{2}{1+(\beta^{(3)})^2}\Big\{\Big(C_{13}^{(3)}(\beta^{(3)})^2 + C_{23}^{(3)}\Big)\Big[r_a\sin\big(\beta^{(3)}\ln r_a\big) - r_2\sin\big(\beta^{(3)}\ln r_2\big)\Big] + \beta^{(3)}\Big(C_{13}^{(3)} - C_{23}^{(3)}\Big)\Big[r_a\cos\big(\beta^{(3)}\ln r_a\big) - r_2\cos\big(\beta^{(3)}\ln r_2\big)\Big]\Big\},$$

$$k_{77} = \left[\frac{\alpha^{(1)}\Big(C_{13}^{(1)} + C_{23}^{(1)}\Big)}{1+(\beta^{(1)})^2} + C_{33}^{(1)}\right]\big(r_1^2 - r_0^2\big) + \alpha^{(2)}\Big(C_{13}^{(2)} + C_{23}^{(2)}\Big)\big[\big(r_2^2\ln r_2 - r_1^2\ln r_1\big)/2 - \big(r_2^2 - r_1^2\big)/4\big] + \left[\alpha^{(2)}C_{13}^{(2)}/2 + C_{23}^{(2)}\right]\big(r_2^2 - r_1^2\big) + \left[\frac{\alpha^{(3)}\big[C_{13}^{(3)} + C_{23}^{(3)}\big]}{1+(\beta^{(3)})^2} + C_{33}^{(3)}\right]\big(r_a^2 - r_2^2\big),$$

$$d_7 = p_0 r_0^2.$$